Polarization domain walls in optical fibres as topological bits for data transmission

M. Gilles[1], P-Y. Bony[1], J. Garnier[2], A. Picozzi[1], M. Guasoni[1,3] and J. Fatome[1,*]

[1]*Laboratoire Interdisciplinaire Carnot de Bourgogne (ICB), UMR 6303 CNRS - Université Bourgogne Franche-Comté, 9 Avenue Alain Savary, BP 47870, 21078 Dijon, France*
[2]*Laboratoire de Probabilités et Modèles Aléatoires, University of Paris VII, 75251 Paris, France*
[3]*Optoelectronics Research Centre, University of Southampton, SO17 1BJ, United Kingdom*
**Corresponding author: jfatome@u-bourgogne.fr*

Domain walls are topological defects which occur at symmetry-breaking phase transitions. While domain walls have been intensively studied in ferromagnetic materials, where they nucleate at the boundary of neighbouring regions of oppositely aligned magnetic dipoles, their equivalent in optics have not been fully explored so far. Here, we experimentally demonstrate the existence of a universal class of polarization domain walls in the form of localized polarization knots in conventional optical fibres. We exploit their binding properties for optical data transmission beyond the Kerr limits of normally dispersive fibres. In particular, we demonstrate how trapping energy in well-defined train of polarization domain walls allows undistorted propagation of polarization knots at a rate of 28 GHz along a 10 km length of normally dispersive optical fibre. These results constitute the first experimental observation of kink-antikink solitary wave propagation in nonlinear fibre optics.

A domain wall (DW) is a type of topological defect that connects two stable states of a physical system. DWs are known to form as a result of a spontaneous symmetry breaking phase transition in a variety of contexts, among which the most popular are magnetism [1], condensed matter [2], spinor Bose-Einstein condensates [3], biological physics (energy transfer in proteins and DNA fluctuations, deoxyribonucleic acid) [2], or particle physics and string theory [4]. They also appear as kinks in close analogy with celebrated kink solutions of the Sine-Gordon equation [2]. DW structures have been widely studied in ferromagnetic materials [1], in which they are known to bind regions in which all spins or magnetic dipoles are aligned in different directions [1-2, 5-7]. Their unique properties are for instance exploited in modern spintronic devices to store or transfer information [9-12]. Despite the fact that DWs have been the subject of numerous studies in ferromagnetism, it is important to note that their equivalent in optics have been poorly exploited so far.

Originally, optical DWs refer to vectorial structures that have been predicted theoretically in the defocusing regime of an isotropic single-mode fibre more than 20 years ago [13-16]. They are fundamentally related to the Berkhoer and Zakharov modulational instability phenomenon [17]. The domain wall corresponds to a localized structure of the kink type that connects two regions of space with different polarizations: In the transition region, the electromagnetic field switches between two stable states with orthogonal circular polarizations -- note that in optical fibres the dynamics is purely temporal and the time along a pulse plays the role of the spatial variable. In this framework, the fast polarization knots leads to two anticorrelated coupled twin-waves for which the strong binding force imposed by cross-phase interaction can compensate for linear and nonlinear impairments induced by normal chromatic dispersion and self-phase modulation, respectively [16]. The polarization distribution is then locked along the propagation within well-defined and robust temporal regions interconnected by polarization domain walls (PDWs) [14].

Owing to their topological nature, a transmission system based on PDWs simply relies on fast polarization switching along the domain edges. As a result, the domains of polarization can be of any time-duration and thus can be encoded individually to carry optical data [18-20]. At variance with classical bright scalar solitons [21], the topological nature of PDWs makes them remarkably robust with respect to external perturbations such as temporal or amplitude fluctuations [13, 19]. This property is fundamentally linked to their topological nature, featured by an energy (Hamiltonian) minimum at both sides of the kink. Therefore, their robustness and attractive properties could find numerous applications in optical communications, all-optical processing, data storage and fibre laser devices. However PDWs remain so far essentially unexplored experimentally.

In 1999, Kockaert *et al.* have experimentally investigated the vectorial modulational instability process in a small piece of one metre isotropic fibre and reported an indirect observation of anticorrelated polarization dynamics [22-23], thus validating the theoretical predictions of Berkhoer and Zakharov. In a different context, antiphase behaviours at nanosecond scale have been also reported in fibre ring laser cavities [24-25] and interpreted recently in terms of PDW-like temporal structures [26-27]. Similar antiphase polarization switching has been also observed by Marconi and co-workers in a vertical-cavity surface-emitting laser [29], which revealed a novel form of dissipative cavity soliton [29-30]. It is important to remind that PDWs reported in laser systems refer to a completely different physics: An optical cavity is inherently a dissipative system [28], which represents a marked distinction with the conservative system considered here.

In contrast to previous works, here we report the first direct observation of PDWs in classical optical fibres commonly used in optical communications. From a broader

perspective, it is found that modern conventional fibres exhibit previously unrevealed distinguished properties, which are shown to support the existence of PDWs in any arbitrary polarization basis. For this reason, the novel class of polarization structures reported here has been qualified as universal PDW. More specifically, we provide a genuine demonstration of the existence of these fundamental structures and exploit their unique topological properties for optical data transmission beyond the nonlinear Kerr-induced limitations of classical normally dispersive fibres. More unexpectedly, we also highlight the robust attraction properties of these entities, which manifest themselves by the spontaneous emergence of synchronized PDWs from a system of incoherent random waves, leading to a phenomenon of polarization segregation, in analogy with the fundamental order–disorder phase transition in ferromagnetic materials. Finally, from a broader perspective, the present observation of PDWs in standard optical fibres raises important questions concerning the limits of validity of the Manakov model for modern standard optical fibres and opens new horizons towards isotropic data transmissions.

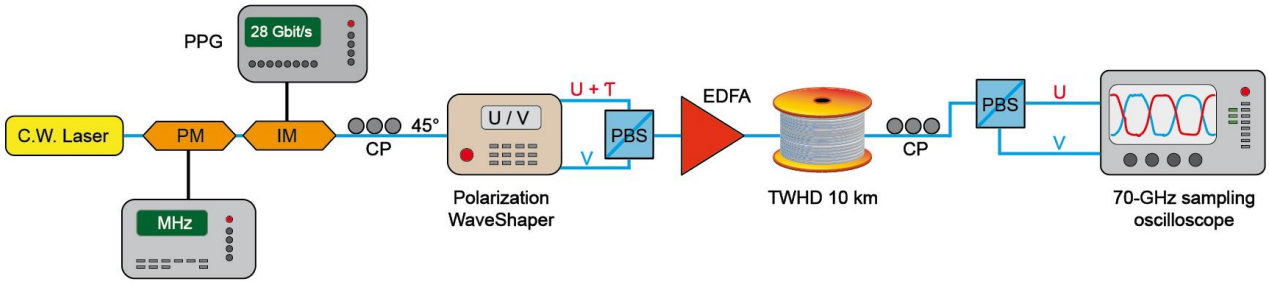

Figure 1. Experimental set-up. In order to generate PDWs, a continuous wave laser (CW) is first phase modulated (PM) to enlarge its spectral linewidth and avoid any Brillouin back-scattering within the fibre. Super-Gaussian pulses are then generated by means of an intensity modulator (IM) driven by a 28-Gbit/s pulse-pattern generator (PPG). The train of square-shaped pulses is then divided into two replicas, delayed by half-a-period (τ) and then orthogonally recombined thanks to a polarization-beam splitter (PBS). Therefore, the resulting signal consists in a train of 28-GHz polarization knots, which confine the energy in well-defined polarization regions. PDWs are amplified by means of an Erbium doped fibre amplifier (EDFA) and injected into a 10-km length of TrueWave High Dispersion fibre (TWHD). At the output of the system, both orthogonal polarization components are characterized in the time domain thanks to a dual-input sampling oscilloscope. CP: polarization controller.

Observation of polarization domain wall solitons

To demonstrate the robustness of polarization domain walls upon propagation in standard optical fibres, we have implemented the experimental set-up depicted in Fig. 1 (see methods for more details). An external cavity laser emitting at λ=1555 nm is first phase modulated so as to enlarge its spectral linewidth in order to prevent any Brillouin back-scattering in the fibre under test. A train of super-Gaussian shaped pulses is generated by means of an intensity Mach-Zehnder modulator driven by a 28-Gbit/s pulse-pattern generator (PPG) delivering a simple periodic 0–1 switching. The resulting signal consists in a train of 30-ps square-shaped pulses at a repetition rate of 14 GHz (duty-cycle 1:2). The signal is then divided into two replicas. One of which is accurately delayed by a half-period and then orthogonally recombined thanks to a polarization-beam splitter (PBS). Therefore, both delayed orthogonal replicas result anticorrelated and consist in a train of 28-GHz polarization knots, which confine the energy in well-defined polarization domains. Note that the corresponding total intensity profile remains almost constant. After amplification by means of an Erbium doped fibre amplifier (EDFA), the PDWs are injected into a 10-km long standard TrueWave fibre characterized by a normal chromatic dispersion $D = -14.5$ ps/nm/km at 1550 nm and a nonlinear Kerr coefficient $\gamma = 2.5$ W^{-1}.km^{-1}. It is important to stress that the fibre under test is non isotropic. It corresponds to a commercially available telecom fibre and therefore exhibits a randomly distributed residual birefringence, as well as an imposed birefringence spinning aimed at controlling such natural birefringence fluctuations (see Methods and Supplemental). Moreover, in the present experiment, the input polarization basis can be arbitrarily selected, which makes our PDWs universal. Indeed, this behaviour is in huge contrast with the isotropic fibre case for which circular polarizations constitute a prerequisite for the formation of DWs [16]. Finally, after transmission through the fibre, both orthogonal polarization components are characterized in the time domain thanks to a second PBS and a dual-input 70-GHz bandwidth sampling oscilloscope.

Figure 2a illustrates the signal monitored at the output of the 10-km long fibre as a function of the injected power when only one polarization component of the domains is injected. Due to the combined effects of chromatic dispersion and self-phase modulation, the output signal is rapidly deteriorated into a complex periodic pattern, which subsequently leads to the development of shock-wave (wave breaking) singularities inherent to the defocusing regime considered here [31-33]. In contrast, as shown in Fig. 2b, when both orthogonally polarized twin-waves are injected into the fibre, the cross-phase modulation interlocks the two signals in a symbiotic fashion [34]. In fact, as a chain of particles trapped in a periodic potential, here the energy contained in each domain is confined due to the perfect balance between chromatic dispersion, self-phase modulation and cross-phase modulation occurring at the domain interfaces. Moreover, it is interesting to notice that in order to maintain such a balance between nonlinear and dispersive effects, an increase of the injected power leads to a reduction of the transition (raising and falling) time between adjacent PDW domains. This also reveals that dispersion plays a key role in the DW structures, which

make them of different nature than those studied in the backward wave configuration [35]. As shown in Fig. 2c, for an input power of 26 dBm, the output intensity profiles recorded on each polarization component of a domain (in red and blue solid lines) remain undistorted compared to the input conditions (in stars), demonstrating the strength of the kink-based domain wall solitons upon propagation impairments. Indeed, when a single component propagates (with half of the total power, in pink dashed-line), the output intensity profile does not fit anymore the initial kink-shaped transition; confirming the high level of impairments induced by the nonlinear scalar transmission. We stress the excellent agreement between the experimental measurements, the numerical simulations (triangles) including experimental parameters, as well as the predicted PDW profile in circles (see methods). Note that similar results have been obtained for different choices of the input polarization basis.

To further assess the quality of the transmitted intensity profiles, we have computed the correlation between the initial and output signals as a function of the injected power. Intuitively, the correlation factor ρ is a number that varies between zero and unity, which denotes the amount of statistical resemblance between the intensity fluctuations of the input and the output waves (see methods for the definition of ρ). As shown in Fig. 2d, the single-component configuration (circles) is characterized by a fast decrease of the correlation function, underlying a dramatic degradation of the propagating wave. In contrast, the robustness of the PDWs (red triangles) allows to maintain, and even improve, the correlation factor to nearly 1, thus revealing a high fidelity of the transmitted kinks & antikinks. This clearly confirms the stability and robustness of the propagating polarization domains.

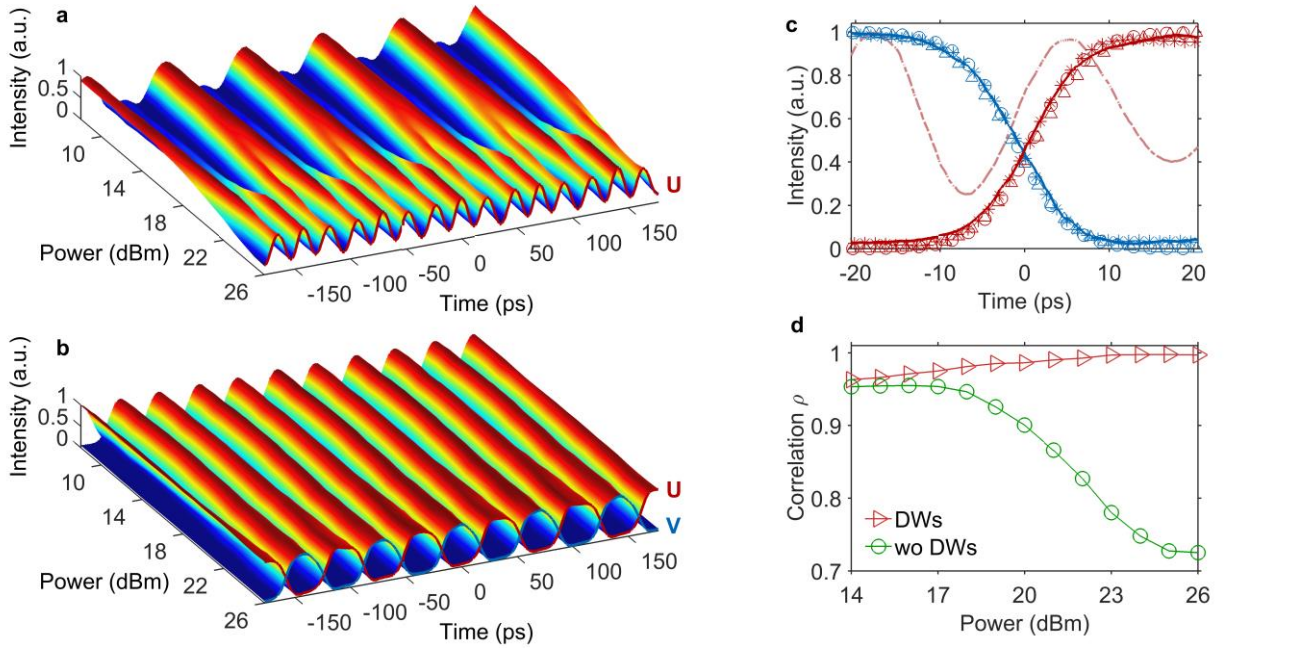

Figure 2. Experimental observation of polarization domain wall solitons. a,b, False-colour plot showing the evolution of the output intensity profile with injected power. Data values are normalized to 1 and mapped to colours linearly **a,** Only one polarization component is injected into the fibre. The output signal is rapidly degraded into a complex periodic pattern **b,** Both anticorrelated twin-waves are injected. PDWs propagate in a symbiotic fashion, confirming the solitonic property of these kink entities. **c,** Output intensity profiles for an injected power of 23 dBm per polarization component. The polarization domains exhibit a robust propagation on both orthogonal components (blue and red solid lines) when compared to the input signal (stars). In contrast, scalar propagation induces a high level of degradation (pink dashed-line). Experimental results are compared with numerical simulations (triangles) and predicted PDW stationary solutions (circles) **d,** Correlation factor ρ between the input and output intensity profiles as a function of the injected power. The single-component configuration (green circles) reveals a fast decrease of the correlation function, highlighting a strong degradation of the propagating wave. In contrast, PDWs (red triangles) preserve a correlation coefficient close to 1, confirming the high robustness and fidelity of the transmitted domains.

Data transmission through polarization domain walls

In order to confirm that the system propagates genuine kink solitons, we have assessed the capability of PDWs to transmit optical data. Indeed, since DWs are solely defined as fast localized polarization knots, they can be of any time-duration and thus may be encoded individually to transmit optical data. In particular, as the signal is no longer periodic, a delayed replica is not sufficient to encode the initial twin-waves. Hence, we used two parallel intensity modulators driven respectively by the $data$ and $\overline{data}$ outputs of the PPG delivering a non-return to zero (NRZ) sequence. Both complementary waves are then properly synchronized and orthogonally recombined in such a way to create the desired PDW sequence. To illustrate the principle, a 40-bit ASCII sequence encoding the acronym of our European Research Council (ERC) project PETAL has been written at a repetition rate of 10 Gbit/s. Note that the data are encapsulated between two extended pre- and post-domains (6 bits) so as to avoid any impairments on the single-edges of the sequence. The encoded PDWs propagate

in a first 25-km long reel of TrueWave fibre before being reamplified and injected in a second span of 25 km.

Figure 3a illustrates the PETAL sequence monitored after 50 km of propagation as a function of the transmitted power when only one of the two twin-waves is injected. In this case, we clearly observe a significant signal degradation leading to a complete loss of the data. These impairments simply result from the detrimental impact of chromatic dispersion and self-phase modulation. In contrast, when both twin-waves propagate simultaneously (Figure 3b), we can clearly observe that the energy remains efficiently locked within each well-defined temporal regions (see Supplementary Movie for direct Lab observation). More specifically, as can be seen in the time domain for an injected power of 24 dBm (Fig. 3c), the PETAL sequence and its anticorrelated replica (red and blue) are ideally preserved after 50 km of propagation, as compared to the single component configuration (green) for which we can observe a complete loss of the transmitted information. These observations confirm the capacity of PDWs to be addressed individually as well as the solitary nature of such kink structures.

Another experimental signature that corroborates the formation of PDWs is provided by spectral measurements. When only one polarization component propagates in the fibre (top of Fig. 3d), the sharp edges in the temporal profile of the initial signal are subjected to a strong self-phase modulation effect. This nonlinear process induces a large amount of chirp characterized by the generation of new frequencies and large spectral broadening. In contrast, thanks to their anticorrelated nature, the PDWs provide an almost ideal chirp compensation between interlocked components, which prevents a significant spectral broadening, as illustrated in the bottom of Fig. 3d. Note that we have also performed a 20-Gbit/s PDWs transmission experiment involving a pseudo-random bit sequence in a 10-km long fibre, whose analysis reveals a well-opened eye-diagram (see Supplementary material). These measurements clearly highlight the ability of PDWs to go beyond the limitations imposed by the nonlinear Kerr effect in normally dispersive fibres.

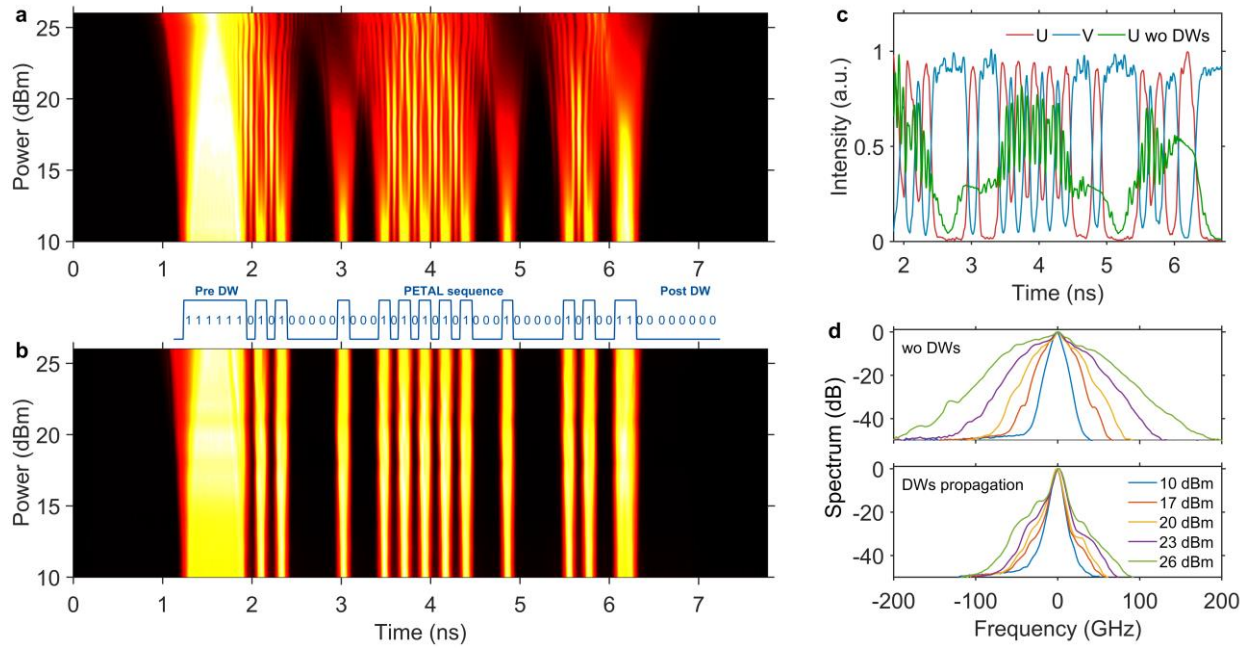

Figure 3. Experimental data transmission through polarization domain walls. a,b, The pseudo-colour plot is made up of a vertical concatenation of the intensity profiles of the 10 Gbit/s PETAL sequence as a function of transmitted power after 50 km of propagation. Data values are normalized from 0 to 1 and are linearly mapped onto the full colour range. **a,** Only one polarization component is injected into the fibre, the data sequence is rapidly degraded. **b,** Polarization domain-wall transmission, the sequence remains ideally preserved. **c,** Intensity profiles monitored at the output of the fibre for an injected power of 24 dBm. The signal and its anticorrelated replica are well conserved after 50 km of propagation, while the single component configuration (green solid line) results fully degraded (see Supplementary Movie for direct Lab observation). **d,** Output optical spectrum as a function of the injected power. On the top, only one single polarization component propagates. The initial signal is therefore subject to a strong self-phase modulation effect, inducing a large spectral broadening. In the bottom, both twin-waves propagate. The polarization domain walls are characterized by an exact chirp compensation at the interface of each domains, which prevent them from large spectral broadening.

Polarization segregation phenomenon

To further highlight the robustness and attracting properties of PDWs, we have explored their spontaneous emergence from an incoherent system of random waves. To this end, the initial signal now consists of an unpolarized noise-source made of two uncorrelated and orthogonally polarized 10-GHz incoherent waves (see methods). This signal is first amplified before injection into a 10-km long span of TrueWave fibre. At the output of the fibre, both orthogonal polarization components are separated thanks to a PBS and characterized in the time domain by means of a 33-GHz bandwidth real-time oscilloscope. Figure 4a illustrates the temporal profiles of the initial signal recorded on both polarization components. We cannot observe any

mutual correlation between the random waves. In contrast, after propagating in the 10-km long optical fibre with an average power of 31 dBm, we can clearly notice in the snapshot of Fig. 4b the emergence of a mutual anticorrelation as well as an outstanding synchronization, which reflect a process of segregation among the orthogonal polarization components. This phenomenon results from the spontaneous emergence of definite temporal regions of polarized domains interconnected among each other by DW structures.

To further assess that a segregation process spontaneously occurs in this system of random waves, we have computed the cross-correlation function μ_{dw} between the orthogonal polarization components. We note that, as described by its definition given in Methods, a negative value of μ_{dw} reveals an anticorrelation, indicating that when one of the polarization component increases, the corresponding orthogonal one decreases, and vice versa. Figure 4c displays the comparison between the input and output cross-correlation traces and confirms the foreseen results. Indeed, the original correlation (black) remains roughly flat and does not reveal any correlated temporal structure. In contrast, when monitored at the output of the fibre (green), we can clearly note a narrow spike centred on the null delay and characterized by a temporal width of 40 ps. Such a dip in the diagram constitutes a signature of the emergence of an anticorrelation among both polarization components, a feature which confirms the spontaneous formation of temporal domains of polarization.

From a broader perspective, this effect of self-organization can be interpreted as a fundamental phenomenon of phase segregation among the orthogonal polarization components. In this sense, it appears in complete analogy with different forms of phase transitions in nature, such as phase segregation of binary fluids [4], or the ferromagnetic order–disorder phase transitions in magnetic systems, as in spinor Bose-Einstein condensates [3]. More precisely, the segregation efficiency of our system can be characterized by the 'order parameter', cross-correlation factor μ_{dw} (see methods). We report in Fig. 4d the results of numerical simulations obtained for our experimental configuration as a function of the total Hamiltonian H, related to the initial degree of incoherence (disorder) of the waves. In analogy with ferromagnetic materials, H plays the role of the temperature (T) in the microcanonical statistical optical ensemble considered here. We observe in Fig. 4d that there exists a critical value of the Hamiltonian, H_c (T_c) here around 0.005, below which the system is cold enough to exhibit a polarization segregation process, whilst above the transition, $H > H_c$, the system becomes too hot to exhibit such a self-ordering phenomenon. This behaviour is similar to the ferromagnetic transition in spin systems: By decreasing H, the system undergoes a transition from a disordered paramagnetic phase (unpolarized, $\mu_{dw} = 0$) towards an ordered ferromagnetic phase characterized by well-defined magnetic domains (PDWs formation $\mu_{dw} \neq 0$). Experimental results corresponding to PDWs transmission of Fig. 2 (coolest state) as well as 10-GHz incoherent wave propagation of Fig. 4 (higher temperature) have been also highlighted with stars in Fig. 4d and provide a good agreement with our numerical simulations.

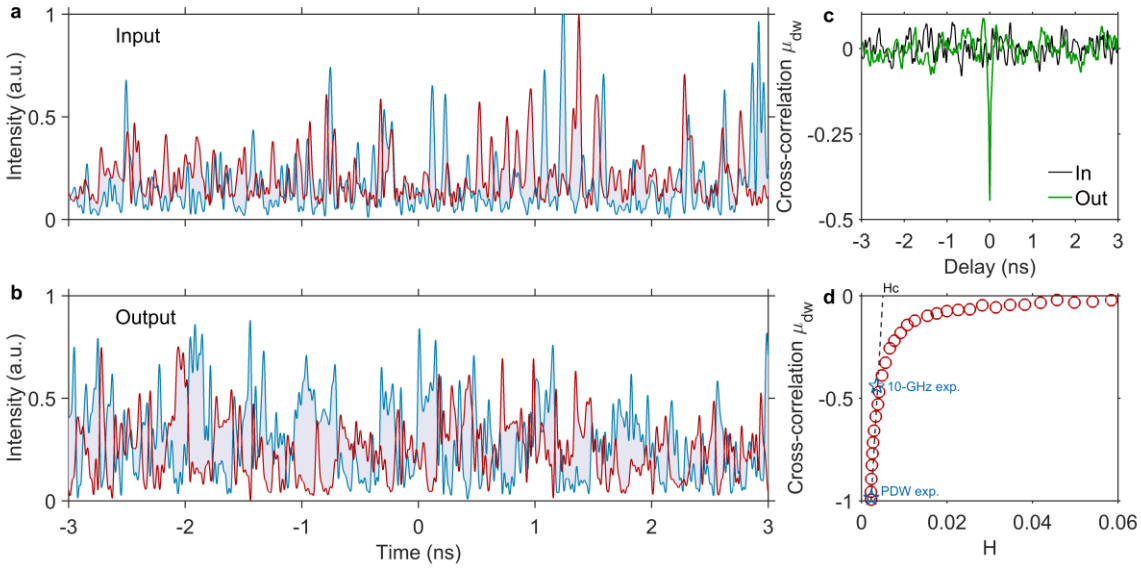

Figure 4. Polarization segregation phenomenon. a, Experimental intensity profile of both orthogonally polarized partially incoherent waves recorded at the input of the fibre for a power of 31 dBm **b,** Corresponding temporal profiles monitored at the output of the fibre. We can observe the emergence of an anticorrelation resulting from the spontaneous emergence of polarization domains, leading to a phenomenon of polarization segregation. **c,** Experimental cross-correlation function between both orthogonal components of the signal calculated at the input (black) and output (green) of the fibre for an average power of 31 dBm. The narrow singularity at zero delay of the output cross-correlation $\mu_{dw}(\tau = 0)$ constitutes the signature of the spontaneous emergence of polarization domains in this system of incoherent waves. **d,** Numerical segregation curves: Cross-correlation factor μ_{dw} as a function of H (temperature): Below some critical value ($H < H_c$), the system undergoes a transition to segregation characterized by an anticorrelation ($\mu_{dw} < 0$) reflecting the spontaneous formation of DWs, in analogy with ferromagnetic materials. Experimental results corresponding to Fig. 2 (PDWs exp.) and Fig. 4b (10-GHz exp.) are also indicated with blue stars.

Discussion

Our study provides a clear experimental evidence of polarization domain walls propagation in conventional telecom optical fibres. We have first injected two anticorrelated orthogonal replicas of a fast square-shape pulse train for which the strong nonlinear coupling induced at the boundaries of both twin-waves acts as a powerful resilience strength to counter-balance the normally dispersive and nonlinear defocusing regime. This strong equilibrium allows to trap the energy in well-defined polarization domains, leading to the undistorted propagation of a 28-GHz train of PDWs along a 10-km long normally dispersive optical fibre. We have also exploited their solitonic properties in order to establish a 10-Gbit/s data transmission beyond the nonlinear Kerr-induced limitations usually imposed in classical optical fibres. More fundamentally, we have confirmed the robust attractive nature of these entities, which manifest themselves by a remarkable phenomenon of polarization segregation, highlighted by the spontaneous emergence of polarized temporal domains in a system of incoherent random waves. This behaviour is interpreted in analogy with the ferromagnetic phase transition, in which a symmetry breaking occurs below a critical value of the energy H_c (temperature) thus bringing the system towards an ordered phase of polarization domains characterized by a non-vanishing value of the order parameter μ_{dw}.

For practical applications, it is important to note that since PDWs are coupled due to an intensity-sensitive cross-polarization interaction, the phase of PDWs can be also encoded within each domain to increase the bit-rate. Moreover, in contrast to classical bright scalar solitons, the topological nature of PDWs make them robust with respect to external perturbations such as timing and amplitude jittering or differential group delay fluctuations. Therefore, their robustness and attracting properties could find numerous applications in optical communications, high-power pulse propagation, all-optical processing, data storage and fibre lasers. The observation of polarization segregation could also find applications for the synchronization of chaotic oscillators and chaos-based optical data transmissions. Nevertheless, due to their anticorrelated nature, it is important to notice that both orthogonal twin-waves are carrying a complementary, yet identical intensity information, which could be a limitation for practical implementation.

It is important to stress that the present observation of PDWs in standard optical fibres goes against the commonly accepted opinion that the Manakov equations accurately model light propagation in random birefringent telecom fibres [35-38]. The Manakov model does not admit PDW soliton states because the cross- and self-phase modulation coefficients coincide. Consequently, the present results raise important questions concerning the validity of the model for modern optical fibres and more interestingly, our results open new horizons towards isotropic data transmissions. We ascribe the present observations to the fast spinning process imposed on modern manufactured fibres, for which complex and rapid spin profiles, such as homogenous or sinusoidal spinning, lead to an effective cancelling of residual birefringence [39-45]. This spinning effect then turns randomly birefringent fibres into a new type of fibres whose behaviour and properties are at the frontier between the so far traditional Manakov fibres and isotropic-like fibres (see methods), which allows for the existence of universal PDWs propagation in any arbitrary polarization basis.

We should then expect that the performance of PDWs transmission would be even improved in the case of an off-spooled or straight-line installed fibres for which the residual birefringence induced by the bending is hence minimized [39]. Furthermore, our results can easily be extended into the spatial domain in bimodal fibres for spatial-division multiplexing applications [46]. In this case, the propagating domains would manifest themselves by a rapid beating of energy between two modes, which enables the possibility to encode information on the modal components of the waves instead of their intensity profiles.

To conclude, more than 20 years after the theoretical prediction of PDWs by Haelterman & Sheppard [14], here we have reported the first direct experimental demonstration of the existence of these fundamental entities and confirm their solitonic nature. More generally, these results can be considered as the first experimental evidence of symbiotic self-organization processes in optical fibres and more importantly as the first kink-type soliton transmission in nonlinear fibre optics.

Methods

Experimental set-up. All the experimental implementations are composed of standard off-the-shelf telecom fibres and components. The set-up involved in the propagation of the 28-GHz periodic train of PDWs consists in an external cavity laser from Yenista (TLS) emitting a continuous-wave (CW) centred at λ=1555 nm. This CW is first modulated thanks to a phase modulator (PM) driven by a triple tones radio-frequency (RF) signal (52, 203 and 506 MHz) to enlarge its spectral linewidth so as to push back the Brillouin scattering threshold of fibres under test high above the powers involved in our experiments. The CW is then encoded through a 40-GHz bandwidth intensity modulator from iXBlue photonics driven by a simple 2-bit sequence of 0 and 1 at a bit rate of 28 Gbit/s provided by the electrical multiplexing of two Non-Return-to-Zero (NRZ) pulse-pattern generators from Anritsu (PPG). The resulting signal consists in a train of 30-ps square-shaped pulses (fitting with a 4-order super-Gaussian) at a repetition rate of 14 GHz (duty-cycle 1:2). The rising and falling time of these square-pulses have been measured to 8 ps. This pulse train is then injected at 45° of the axes of a polarization Waveshaper (2000S tunable liquid-crystal based optical filter from Finisar) which, combined to a polarization-beam splitter (PBS) allow us to successively duplicate, finely adjust the delay between both replicas by half-a-period and orthogonally polarization multiplex both complementary pulse trains. Therefore, both delayed orthogonal replicas appear anticorrelated and consist in a 28-GHz orthogonal polarization flip-flopping imposed on a continuous-wave. This train of polarization kinks and antikinks structures is then amplified by means of an Erbium doped fibre amplifier (EDFA from 3S photonics). A polarization controller is used at the input of the fibre to adjust the input state-of-polarization (SOP). However, no influence of the input SOP has been noticed on the temporal profiles of output signals. The PDWs are then injected into a 10-km long TrueWave High Dispersion fibre (TWHD commercially available from OFS). The fibre is characterized by a chromatic dispersion D = –14.5 ps/nm/km at 1550 nm, a polarization mode dispersion of 0.02 ps/km$^{1/2}$, losses of 0.2 dB/km and a nonlinear Kerr coefficient γ = 2.5 W^{-1}.km^{-1}. At the output of the system, both orthogonal replicas are polarization

demultiplexed by means of a polarization controller combined to a second PBS. This demultiplexing operation allows us to decompose the output PDWs on the initial polarisation basis so as to characterize both replicas in the time domain thanks to a dual-input 70-GHz bandwidth photodiode (from u2t) and an electrical sampling oscilloscope (Keysight DCA). What we call the 'initial polarization basis' refers to the basis recovered by switching off one polarization component at the input of the fibre and maximize or minimize the energy of the other component on one axis of the PBS at the system output.

Data transmission through PDWs. The phase modulated CW is split in two arms by means of a polarization maintaining 50:50 coupler. Both replicas are then intensity modulated thanks to two parallel intensity modulators from iXBlue photonics. Each modulator is driven by the phase-matched $data$ and $\overline{data}$ sequence delivered by our 10-Gbit/s NRZ pulse-pattern generator. We can notice that this PDWs transmitter could be directly implemented by means of a high-bandwidth electro-optic polarization modulator. The emitted data sequence was chosen as the 40-bit long ASCII code of the ERC project acronym PETAL (0101000001000101010101000 100000101001100). The sequence was encapsulated between two extended polarization domains (6 bits of 0 on one arm and 6 bits of 1 on the other) so as to avoid any impairments on the single edges of the PETAL sequence. Both anticorrelated waves are then carefully synchronized in the time domain and orthogonally recombined by means of the 2000S polarization Waveshaper combined to a PBS. The encoded PDWs are then amplified thanks to a 33-dBm EDFA and propagate in a first fibre spool of 25 km of TrueWave fibre before being reamplified by a second EDFA and injected into a second span of 25 km. At the output of the transmission line, the PDWs are characterized in the time domain by using the same procedure as that detailed in the previous study.

Polarization segregation phenomenon. The combination of anticorrelated pulse trains used to study PDW propagation has been substituted by two uncorrelated incoherent waves. The injected signal consists in an amplified spontaneous noise emission (ASE) generated from an Erbium-based optical source operating in the telecom C-band. This ASE signal is then carved in the spectral domain with a 10-GHz bandwidth and simultaneously split in two orthogonal replicas by means of the 2000S polarization Waveshaper. The resulting waves are then decorrelated in time through the propagation in different paths of fibres (1 km of SMF) and recombined with orthogonal polarizations thanks to two polarization controllers and a PBS. Both incoherent waves are amplified thanks to a 33-dBm EDFA from 3S photonics before injection into a 10-km long span of TrueWave fibre. At the output of the fibre, both orthogonal incoherent waves are polarization demultiplexed by means of a polarization controller combined to a PBS. As previously mentioned in the experimental set-up section, the initial polarization basis is finely retrieved by maximizing (minimizing) one or the other polarization components on the output PBS in the absence (presence) of the second wave at the system input. In order to characterize the incoherent waves in the temporal domain, we directly monitored their intensity profiles by means of two finely balanced channels of a 33-GHz real-time oscilloscope associated with two 70-GHz bandwidth photodiodes from u2t.

Numerical modelling. There exist some consensus that light propagation in randomly birefringence Telecom fibres is accurately modelled by the set of Manakov equations [35-38]. In these coupled equations, the ratio between self- and cross-phase modulation effects is unity and the effective Kerr nonlinearity is reduced by a factor 8/9 so as to take into account for fast and random birefringence fluctuations, which lead to a homogeneous distribution of the polarization states on the Poincaré sphere. Nevertheless, as the formation of polarization domain walls occurs when cross-phase modulation exceeds the self-phase modulation effect, a ratio between the cross- and self-phase modulation coefficients larger than 1 is required for their existence [13]. In order to provide an intuitive phenomenological description of our experimental observations, we have implemented the following model where u and v correspond to orthogonal polarization components of the field in an arbitrary polarization basis:

$$\begin{cases} i\dfrac{\partial u}{\partial z} = \dfrac{\beta_2}{2}\dfrac{\partial^2 u}{\partial t^2} - \gamma(|u|^2 + C_{XPM}|v|^2)u, \\ i\dfrac{\partial v}{\partial z} = \dfrac{\beta_2}{2}\dfrac{\partial^2 v}{\partial t^2} - \gamma(|v|^2 + C_{XPM}|u|^2)v \end{cases} \quad (1)$$

where z corresponds to the propagation coordinate, t the local time in the reference frame of the fields, β_2 the chromatic dispersion coefficient (normal dispersion regime is required for the existence of PDWs [13]), γ the Kerr coefficient and C_{XPM} denotes for the ratio between cross- and self-phase modulation coefficients. Linear propagation losses have been neglected for simplicity. Note that despite its apparent simplicity, this phenomenological model describes several properties of our experimental observations. In particular, it admits stable PDW solitons for $C_{XPM} > 1$, and provides an excellent agreement with the experimental results reported in Fig. 2c for a cross-phase modulation coefficient of $C_{XPM} = 1.3$ and different choices of the experimental polarization basis.

These observations question the validity of the usual Manakov model commonly accepted to describe light propagation in standard Telecom optical fibres. As will be discussed below, this unexpected finding results from the implementation of fast spinning profiles on the birefringence fibres axis during the drawing stage of the manufacturing process of modern spun fibres [39-45]. A commonly used spin profile exhibits a sinusoidal shape, for which the birefringence axes of the fibre rotates back and forth according to $\alpha(z) = \alpha_0 sin(2\pi\, z/L_{spin}) + \eta(z)$, where the spatial period of the spinning process, L_{spin}, is the smallest spatial scale of the problem, typically of the order of few metres, while α_0, the amplitude of the spinning can be as large as hundreds of rad/m [45]. The stochastic contribution $\eta(z)$ is unavoidable since it originates in natural fibre birefringence fluctuations. The random function $\eta(z)$ is of zero mean and characterized by a correlation function $R(z/L_c)$, L_c being the correlation length of birefringence fluctuations. Note that the random contribution can be considered as a perturbation with respect to the imposed sinusoidal spinning, $\eta_0 = \sqrt{<\eta^2>} \ll \alpha_0$.

By using a homogenization theorem [47] and the Jacobi expansion $e^{2i\alpha_0 \sin(2\pi z/L_{spin})} = J_0(2\alpha_0) + \sum_{n=1}^{\infty} J_n(2\alpha_0)[e^{inkz} + (-1)^n e^{-inkz}]$, light propagation in the fibre can be shown to be described by the following reduced model:

$$\begin{cases} i\dfrac{\partial \tilde{u}}{\partial z} = \dfrac{\beta_2}{2}\dfrac{\partial^2 \tilde{u}}{\partial t^2} - \dfrac{\Delta\beta}{2}J_0(2\alpha_0)\tilde{v} + \varepsilon\tilde{u} - \dfrac{2\gamma}{3}(|\tilde{u}|^2 + 2|\tilde{v}|^2)\tilde{u}, \\ i\dfrac{\partial \tilde{v}}{\partial z} = \dfrac{\beta_2}{2}\dfrac{\partial^2 \tilde{v}}{\partial t^2} - \dfrac{\Delta\beta}{2}J_0(2\alpha_0)\tilde{u} - \varepsilon\tilde{v} - \dfrac{2\gamma}{3}(|\tilde{v}|^2 + 2|\tilde{u}|^2)\tilde{v} \end{cases} \quad (2)$$

where $\tilde{u}$ and $\tilde{v}$ refer to circular polarization components of the field, $\Delta\beta$ the propagation constant difference between the axes, J_0(x) the zero-th order Bessel function of the first kind [44], and $\varepsilon(z) = \partial_z\eta(z)$, models the random contribution of the birefringence. As revealed by Eqs. 2, the fast fibre spinning introduces a controlled polarization-mode coupling through an effective beat length, $L_B^{eff} = 2/[\Delta\beta\, J_0(2\alpha_0)]$. In our experiments, the nonlinear and dispersive effects act in the km range, while the correlation length of polarization fluctuations ($L_c \sim 50m$) is typically much shorter than the effective beat length, $L_c \ll L_B^{eff}$, with L_B^{eff} of few hundred metres. In this way, random birefringence fluctuations are essentially averaged out during the propagation. To properly understand such an averaging process, we follow the general procedure originally introduced by Wai and Menyuk [37], to describe the distribution of the Stokes vector of the optical field over the Poincaré sphere through the analysis of the effective birefringence (L_B^{eff}) and random birefringence (L_c) effects. Making use of the diffusion approximation theorem [48], we derived a Fokker-Planck-like equation governing

the evolution of the probability density of the Stokes vector on the surface of the Poincaré sphere. This equation reveals two fundamental limiting cases. First-of-all, when $\left(L_B^{eff}\right)^2/(\psi(\eta_0)L_c) \ll L_{nl}$, with $\psi(\eta_0) = 2\,exp(-4\eta_0^2)\int_0^\infty sinh^2\left(2\eta_0^2 R(s)\right)ds$, then the Stokes vector becomes uniformly distributed over the Poincaré sphere before the onset of nonlinear effects. In this way, the averaging of the nonlinear terms lead to the usual Manakov system [37-38]. On the other hand, when $\left(L_B^{eff}\right)^2/(\psi(\eta_0)L_c) \gg L_{nl}$, it is possible to show that the optical field is governed by a set of equations formally analogous to those of a low birefringent, or isotropic fibre, with an effective birefringence length, $L_B^{eff}\exp(2\eta_0^2)$. Our experimental observations place modern manufactured optical fibres between these two limits. Unfortunately, the evolution of the optical field in this intermediate regime cannot be described by deterministic equations, but by a set of coupled stochastic nonlinear Schrödinger equations. We have also studied the robustness of such reduced averaged equations with respect to noise perturbations. The analysis revealed that, thanks to the fast spinning of the fibre birefringence axes, noise fluctuations of velocity matching between the orthogonal polarization components can be completely averaged out, which has the effect to dramatically reduce the detrimental impact of group-delay noise on signal propagation. See the Supplemental material for a detailed discussion of the theoretical developments.

Hamiltonian properties. The system of Eqs. 1 conserves several important quantities, the power of each wave, $N_j = \int |j|^2\,dt$, $j = u, v$, and the Hamiltonian, $H = E + H_{nl} + H_{XPM}$, with the linear $E = \beta_2/2\sum_{j=u,v}\int|\partial_t j|^2 dt$, nonlinear $H_{nl} = \gamma/2\sum_{j=u,v}\int|j|^4 dt$, and interaction $H_{XPM} = C_{XPM}\gamma\int|u|^2|v|^2 dt$, energy contributions. Note that in statistical mechanics, the energy H usually provides a measure of the 'amount of excitation' in the system (temperature in ferromagnetic materials for instance). In the weakly nonlinear regime ($E \gg H_{nl,XPM}$), the energy per particle *E/N* provides an appropriate measure of the amount of incoherence, which is related to the normalized spectral bandwidth of the waves, in analogy with kinetic gas theory [49].

Stationary solutions. Since no analytical solution exists for the temporal profile of polarization domain walls, we have numerically computed the stationary solutions of Eqs. 1 in order to compare them to our experimental results of Fig. 2c. To this end, a tangent-hyperbolic ansatz is numerically injected into the set of coupled Eqs. 1. These equations are then resolved with a standard split-step Fourier algorithm on 5 nonlinear lengths L_{nl}, defined as $1/\gamma P$, P the total average power. The propagating intensity profiles on each polarization component are then temporally averaged along the whole fibre length while the resulting rooting square provides a new set of initial conditions for Eqs. 1. This process is then repeated until the optical fields converge to a PDW soliton stationary solution (typically 50 iterations).

Intercorrelation. In order to calculate the correlation coefficient ρ between the input and output signals in Figs. 2d, the intensity profiles of the input and output polarization components $U_{in} = |u_{in}(t)|^2$ and $U_{out} = |u_{out}(t)|^2$ were recorded on the oscilloscope and the linear correlation was computed using the following expression:

$$\rho(U_{in}, U_{out}) = \frac{\langle U_{in}U_{out}\rangle}{\sqrt{\langle U_{in}^2\rangle\,\langle U_{out}^2\rangle}} \qquad (3)$$

where angle brackets denotes the temporal averaging over the intensity profile.

The correlation function reported in Fig. 4c denotes the cross-correlation among both output orthogonal polarization components $U(t) = |u_{out}|^2$ and $V(t) = |v_{out}|^2$:

$$\mu_{dw}(U,V)(\tau) = \frac{\langle U(t)\,V(t-\tau)\rangle - \langle U(t)\rangle\langle V(t)\rangle}{\sqrt{var[U(t)]\;var[V(t)]}} \qquad (4)$$

where *var(x)* denotes the variance of x. Note that the above correlators solely involve the intensities of the waves and that they are related to the general notion of second-order coherence theory of classical vector fields. It is important to notice that $\mu_{dw}(U,V) < 0$ reveals an anticorrelation, indicating that when U increases, V decreases and vice versa. This type of correlation function has been recently used for instance to characterize noise and wavelength correlation properties of octave-spanning supercontinuum in ref. [50].

The numerical segregation curve reported in Fig. 4d has been obtained through Eqs. 1 by computing μ_{dw} for τ=0 after propagation throughout the fibre (output of the system) for different values of the Hamiltonian H, which is a conserved quantity during propagation. The value of H for each individual simulations has been varied by considering different spectral bandwidths of the initial incoherent waves, whose spectra are Gaussian-shaped with random spectral phases -- the waves exhibit Gaussian statistics with temporal fluctuations that are statistically stationary in time. Accordingly, irrespective of the value of H, μ_{dw} = 0 for the initial condition at z = 0. If $H < H_c$ ($H > H_c$), the segregation process (does not) takes place, and $\mu_{dw} \neq 0$ ($\mu_{dw} = 0$) after propagation throughout the fibre. Minimum values of H have been then reached by progressively adding a CW components in the incoherent wave so as to develop classical polarization modulational instability (PMI). Decreasing further the temperature of the waves was finally obtained by progressively seeding the MI process until injection of the theoretical stationary solutions of PDWs.

Thermodynamic approach and phase transition. The phenomenon of polarization segregation has a thermodynamic origin, in the sense that it is thermodynamic advantageous for the system to exhibit polarization segregation, because this entails an increase of the amount of disorder. This counter-intuitive phenomenon can be interpreted by recalling that the soliton realizes the minimum of the energy (Hamiltonian): The system then relaxes toward the state of lowest energy, which allows the small-scale fluctuations to store the maximum amount of kinetic energy (i.e., "disorder"). Indeed, the linear (kinetic) energy E provides a natural measure of the amount of disorder [49]: During the propagation E increases ($\Delta E > 0$) at the expense of a reduction of the interaction energy ($\Delta H_{XPM} < 0$), while the total energy H is kept constant. Note however that the one-dimensional system considered here does not exhibit a genuine thermalization [49], so that the segregation process occurs far from thermodynamic equilibrium.

References

1. Weiss, P. L'hypothèse du champ moléculaire et la propriété ferromagnétique. *J. Phys. Rad.* **6**, 661-690 (1907).
2. Reichl, L., *A modern course in statistical physics,* Wiley-VCH Verlag GmbH (2004).
3. Dauxois, T. & Peyrard, M., *Physics of solitons*, Cambridge University Press (2010).
4. Stamper-Kurn, D.N. & Ueda, M. Spinor Bose gases: Symmetries, magnetism, and quantum dynamics. *Rev. Mod. Phys.* ***85***, 1191-1244 (2013).
5. Weinberg, S. *The Quantum Theory of Fields*, Vol. 2., Cambridge University Press (1995).
6. Parpia, D.Y., Tanner, B.K. & Lord, D.G. Direct optical observation of ferromagnetic domains. *Nature* **303**, 684-685 (1983).
7. Kosevich, A.M. Dynamical and topological solitons in ferromagnets and antiferromagnets. In *Solitons* (Elsevier, 1986).
8. Unguris, J., Celotta, R.J. & Pierce, D.T. Observation of two different oscillation periods in the exchange coupling of Fe/Cr/Fe(100). *Phys. Rev. Lett.* **67**, 140-143 (1991).
9. Allwood, D.A. *et al.* Magnetic domain-wall logic. *Science* **309**, 1688-1692 (2005).

10. Parkin, S.S., Hayashi, M. & Thomas, L. Magnetic domain-wall racetrack memory. *Science* **320**, 190-194 (2008).
11. Currivan-Incorvia, J.A. *et al.* Logic circuit prototypes for three-terminal magnetic tunnel junctions with mobile domain walls. *Nat. Commun.* **7**:10275 (2016).
12. Tetienne, J.P. *et al.* The nature of domain walls in ultrathin ferromagnets revealed by scanning nanomagnetometry. *Nat. Commun.* **6**:6733 (2015).
13. Haelterman, M. & Sheppard, A.P. Bifurcation of the dark soliton and polarization domain walls in nonlinear dispersive media. *Phys. Rev E* **49**, 4512-4518 (1994).
14. Haelterman, M. & Sheppard, A.P. Vector soliton associated with polarization modulational instability in the normal-dispersion regime. *Phys. Rev E* **49**, 3389-3399 (1994).
15. Malomed, B.A. Optical domain walls. *Phys. Rev. E* **50**, 1565-1571 (1994).
16. Sheppard, A.P. & Haelterman, M. Polarization-domain solitary waves of circular symmetry in Kerr media. *Opt. Lett.* **19**, 859-861 (1994).
17. Berkhoer, A.L. & Zakharov, V.E. Self-excitation of waves with different polarizations in nonlinear media. *Sov. Phys. JETP* **31**, 486-490 (1970).
18. Haelterman, M. Polarisation domain wall solitary waves for optical fibre transmission. *Electron. Lett.* **30**, 1510-1511 (1994).
19. Haelterman, M. Colour domain wall solitary waves for nonreturn-to-zero transmission scheme. *Electron. Lett.* **31**, 741-742 (1995).
20. Wabnitz, S. Cross-polarization modulation domain wall solitons for WDM signals in birefringent optical fibers. *IEEE Photon. Technol. Lett.* **21**, 875-877 (2009).
21. Gordon, J.P. & Haus, H.A. Random walk of coherently amplified solitons in optical fiber transmission. *Opt. Lett.* **11**, 665-667 (1986).
22. Kockaert, P., Haelterman, M., Pitois, S. & Millot, G. Isotropic polarization modulational instability and domain walls in spun fibers. *Appl. Phys. Lett.* **75**, 2873-2875 (1999).
23. Gutty, F. *et al.* Generation and characterization of 0.6-THz polarization domain-wall trains in an ultralow-birefringence spun fiber. *Opt. Lett.* **24**, 1389-1391 (1999).
24. Quinton, L.W. & Roy, R. Fast polarization dynamics of an erbium-doped fiber ring laser. *Opt. Lett.* **21**, 1478-1480 (1996).
25. Williams, Q.L., García-Ojalvo, J., & Roy. R. Fast intracavity polarization dynamics of an erbium-doped fiber ring laser: Inclusion of stochastic effects. *Phys. Rev. A*, **55**, 2376-2386 (1997).
26. Zhang, H., Tang, D.Y., Zhao, L.M. & Wu, X. Observation of polarization domain wall solitons in weakly birefringent cavity fiber lasers. *Phys. Rev. B* **80**, 052302 (2009).
27. Lecaplain, C., Grelu, P. & Wabnitz, S. Polarization-domain-wall complexes in fiber lasers. *J. Opt. Soc. Am. B* **30**, 211-218 (2013).
28. Tsatourian, V. *et al.* Polarisation Dynamics of Vector Soliton Molecules in Mode Locked Fibre Laser. *Sci. Rep.* **3**:3154 (2013).
29. Marconi M., Javaloyes J., Barland S., Balle S. & Giudici M. Vectorial dissipative solitons in vertical-cavity surface-emitting lasers with delays. *Nat. Photon.* **9**, 450-455 (2015).
30. Jang, J.K., Erkintalo, M., Coen, S. & Murdoch, S. Temporal tweezing of light through the trapping and manipulation of temporal cavity solitons. *Nat. Commun.* **6**:7370 (2015).
31. Tomlinson, W.J., Stolen R.H. & Johnson, A.M. Optical wave breaking of pulses in nonlinear optical fibers. *Opt. Lett.* **10**, 467-469 (1985).
32. Rothenberg, J.E. & Grischkowsky, D. Observation of the formation of an optical intensity shock and wavebreaking in the nonlinear propagation of pulses in optical fibers. *Phys. Rev. Lett.* **62**, 531 (1989).
33. Fatome, J. *et al.* Observation of Optical Undular Bores in Multiple Four-Wave Mixing fibers. *Phys. Rev. X* **4**, 021022 (2014).
34. Gilles, M. *et al.* Data transmission through polarization domain walls in standard telecom optical fibers. Presented in the summer school *Spatiotemporal Complexity in Nonlinear Optics (SCNO)*, 31 Aug. – 4 Sept. 2015, Como, Italy.
35. Pitois, S., Millot, G. & Wabnitz, S. Polarization domain wall solitons with counterpropagating laser beams. *Phys. Rev. Lett.* **81**, 1409-1412 (1998).
36. Manakov, S.V. On the theory of two dimensional stationary self-focusing of electromagnetic waves. *Sov. Phys. JETP* **38**, 248-253 (1974).
37. Wai P.K.A. & Menyuk, C.R. Polarization mode dispersion, decorrelation, and diffusion in optical fibers with randomly varying birefringence. *IEEE J. Lightw. Technol.* **14**, 148-157 (1996).
38. Marcuse, D., Menyuk, C.R. & Wai, P.K.A. Application of the Manakov-PMD equation to studies of signal propagation in optical fibers with randomly varying birefringence. *IEEE J. Lightw. Technol.* **15**, 1735-1746 (1997).
39. Geisler, T. Low PMD transmission Fibers. *In European Conference on Optical Communications (ECOC)*, Mo.3.3.1 (2006).
40. Barlow, A.J., Ramskov-Hansen, J.J. & Payne D.N. Birefringence and polarization mode-dispersion in spun singlemode fibers. *Appl. Opt.* **20**, 2962-2968 (1981).
41. Li, M.J. & Nolan, D.A. Fiber spin-profile designs for producing fibers with low polarization mode dispersion. *Opt. Lett.* **23**, 1659-1661 (1998).
42. Palmieri, L. Polarization Properties of Spun Single-Mode Fibers *IEEE J. Lightw. Technol.* **24**, 4075-4088 (2006).
43. Galtarossa, A., Palmieri, L. & Sarchi, D. Measure of Spin Period in Randomly Birefringent Low-PMD Fibers. *IEEE Photon. Technol. Lett.* **16**, 1131-1133 (2004).
44. Nolan, D.A., Chin, X. & Li, M.J. Fibers With Low Polarization-Mode Dispersion. *IEEE J. Lightw. Technol.* **22**, 1066-1088 (2004).
45. Palmieri, L., Geisler, T. & Galtarossa, A. Effects of spin process on birefringence strength of single-mode fibers. *Opt. Express* **20**, 1-6 (2012).
46. Pitois, S., Millot, G., Grelu, P. & Haelterman, M. Generation of optical domain-wall structures from modulational instability in a bimodal fiber. *Phys. Rev E* **60**, 994 (1999).
47. Kurzweil, J. & Jarnık, J. Limit processes in ordinary differential equations. *Journal of Applied Mathematics and Physics* **38**, 241-256 (1987).
48. Fouque, J.P., Garnier, J., Papanicolaou, G. & Solna, K. Wave *Propagation and Time Reversal in Randomly Layered Media*, (Springer, 2007), see chap. 6 (theorem 6.1)
49. Picozzi, A., *et al.,* Optical wave turbulence: Toward a unified nonequilibrium thermodynamic formulation of statistical nonlinear optics. *Phys. Reports* **542**, 1-132 (2014).
50. Godin, T. *et al.,* Real time noise and wavelength correlations in octave-spanning supercontinuum generation. *Opt. Express* **21**, 18452-18460 (2013).

Acknowledgements

J.F. acknowledges the financial support from the European Research Council under the European Community's Seventh Framework Programme (ERC starting grant PETAL n°306633, Polarization condEnsation for Telecom AppLications). We also thank the Conseil Régional de Bourgogne Franche-Comté under the PARI Action Photcom program as well as the Labex ACTION program (ANR-11-LABX-0001-01). We thank Doc. S. Pitois and T. Geisler from ofs for fruitful discussions, E. Paul for illustrations as well as S. Pernot, V. Tissot and B. Sinardet for electronic developments. M.G. acknowledges support from the European Commission through Marie Skodowska-Curie Fellowships: IF project AMUSIC – 02702.

Author contributions

J. F., P-Y. B. and M. G. performed the experiments. Mass. G., J. G. and A. P. contributed to the theoretical and numerical analysis. All authors participated in the analysis of the results. J. F wrote the paper and supervised the overall project.

Additional information

Supplementary information is available online. The data that support the plots within this paper and other findings of this study are available from the corresponding author upon reasonable request. Correspondence and requests for materials should be addressed to J.F.

Competing financial interests

The authors declare no competing financial interests.